CDK9 regulates neointima formation following vascular injury by targeting the transcription factor Twist1

LIQING YU, XIAOXIA ZHOU, JIAFENG CHEN, MENGXIANG LI, RUIYING WANG, GANG LI and JUN WU

Fujian Branch of National Clinical Research Center for Cardiovascular Diseases, Xiamen Cardiovascular Hospital of Xiamen University, School of Medicine, Xiamen, Fujian 361000, P.R. China

Received March 24, 2026; Accepted November 5, 2026

DOI: 10.3892/ijmm.2026.6063

Abstract. Restenosis is a major limiting factor of percutaneous coronary intervention, accompanied by abnormal proliferation, migration and phenotypic switching of vascular smooth muscle cells (VSMCs). As a key component of the positive transcription elongation factor b complex, cyclin-dependent kinase 9 (CDK9) phosphorylates RNA polymerase II (RNA Pol II) and regulates various genes that are involved in the regulation of diverse cellular processes, including cell proliferation. The present study aimed to investigate whether and how CDK9 regulates vascular remodeling after injury in mice. Carotid artery ligation was performed in C57BL/6J mice, and cultured VSMCs were treated with platelet-derived growth factor-BB, iCDK9, Thal-SNS-032, harmine or CDK9-overexpressing recombinant adenovirus. Neointimal formation, proliferation, migration and phenotypic switching were examined by histological quantification, western blotting, reverse transcription-quantitative PCR, 5-ethynyl-2'-deoxyuridine incorporation, wound-healing and immunofluorescence assays, and the mechanism was explored by RNA-sequencing, chromatin immunoprecipitation and luciferase reporter assays. The results revealed a notable upregulation of CDK9 and the phosphorylation of RNA Pol II at Ser2 in VSMCs during neointimal hyperplasia following carotid artery injury, and the neointimal formation could be markedly ameliorated by a CDK9 inhibitor. Furthermore, overexpression of CDK9 promoted the phenotypic switching, proliferation and migration of VSMCs *in vitro*, whereas inhibition of CDK9 produced the opposite results. Furthermore, CDK9 exerted its biological function by directly targeting the transcription factor Twist1, which is a key inducer of epithelial-mesenchymal transition that has been widely implicated in the pathological progression of cardiovascular diseases. Additionally, application of the Twist1 inhibitor harmine markedly abolished the function of CDK9 in promoting the phenotypic switching, proliferation and migration of VSMCs *in vitro*. In conclusion, the present study explored the function of CDK9 in vascular injury-induced neointimal hyperplasia and established that CDK9 may exert direct targeting regulation on the transcription factor Twist1 within this pathological cascade.

Correspondence to: Dr Gang Li or Dr Jun Wu, Fujian Branch of National Clinical Research Center for Cardiovascular Diseases, Xiamen Cardiovascular Hospital of Xiamen University, School of Medicine, 2999 Jinshan Road, Huli, Xiamen, Fujian 361000, P.R. China
E-mail: ligang@xmu.edu.cn
E-mail: wujun229@xmu.edu.cn

Key words: neointimal formation, vascular smooth muscle cell, cyclin-dependent kinase 9, phenotypic switching, Twist1

Introduction

Cardiovascular diseases are the leading cause of human morbidity and mortality worldwide (1-3). In recent decades, the incidence of vascular stenosis-related diseases, particularly coronary heart disease, has been increasing, thus threatening human health (4-7). Clinically, percutaneous coronary intervention (PCI) is a well-established and effective method for the treatment of coronary artery disease (8-11); however, vascular restenosis is currently a common complication (12-14). Previous studies have reported that the neointima formation primarily driven by excessive proliferation and migration of vascular smooth muscle cells (VSMCs) serves a vital role in restenosis (15-17).

VSMCs are a major component of blood vessels, which serve an important role in maintaining the physiological functions of blood vessels (18). VSMCs are not terminally differentiated, and exhibit phenotypic and functional plasticity in response to microenvironmental cues (16,18-20). Under normal physiological conditions, VSMCs located in the media of the vascular wall exhibit a contractile phenotype, and possess low proliferative and migratory capacities (21,22). The quiescent contractile phenotype of VSMCs is characterized by abundant expression of contractile phenotype-associated genes, including myocardin, calponin 1 (CNN1), α-smooth muscle actin (α-SMA), transgelin (SM22α) and myosin heavy chain 11 (23,24). In response to vascular injury or other pathological stimuli, VSMCs switch from a contractile phenotype to a dedifferentiated synthetic phenotype, which is characterized by a notable decrease in contractile gene expression, as well as high proliferative and migratory abilities (25-27). Synthetic

VSMCs proliferate and migrate to the vascular intima, which is accompanied by the secretion and deposition of extracellular matrix (ECM) factors, such as Aggrecan and Versican, resulting in continuous production of neointima (28-30). Therefore, the phenotypic switching of VSMCs has a vital role in neointima formation and vascular stenosis, and deciphering the molecular mechanisms governing VSMC phenotypic switch is important for the development of novel options for interventions in vascular remodeling after injury.

As a key component of the positive transcription elongation factor b (P-TEFb) complex, cyclin-dependent kinase 9 (CDK9) differs from other CDK family members in that it has minimal effects on regulating the cell cycle (31,32). Instead, it mainly regulates gene transcription through phosphorylating the C-terminal domain (CTD) of RNA polymerase II (RNA Pol II) at Ser2 [phosphorylated (p)-Ser2], which is critical for RNA synthesis (33,34). The function of CDK9 in cancer and acquired immunodeficiency syndrome has been well studied, and an increasing number of studies have revealed that CDK9 is also involved in cardiovascular diseases (35-40). For example, under pro-hypertrophic stimuli, CDK9 can be recruited to promoter regions of hypertrophic genes by other transcription factors, such as bromodomain-containing 4 and the p300/GATA-binding protein 4 (GATA4) complex, and then increase p-Ser2 and facilitate the transcription level of target genes, such as ANF and ET-1, leading to cardiomyocyte proliferation and cardiac hypertrophy (35). Additionally, the elevation of CDK9 in the serum of patients with atherosclerosis (AS) or pulmonary arterial hypertension (PAH) has been observed (40-42). Although several studies have reported that CDK9 can promote the development of AS and PAH by regulating the proliferation and phenotypic switching of VSMCs, its role and underlying molecular mechanism in arterial injury and subsequent neointimal formation remain poorly understood. The present study aimed to address this issue and to further verify whether Twist1 acts as a downstream effector of CDK9 during vascular remodeling.

The current study aimed to investigate the role and underlying mechanism of CDK9 in vascular injury-induced neointimal hyperplasia both *in vitro* and *in vivo*. Specifically, the present study had the following aims: i) To determine whether CDK9 expression and its kinase activity (reflected by RNA Pol II Ser2 phosphorylation) are altered in vascular smooth muscle cells following vascular injury; ii) to examine the effects of CDK9 inhibition, knockdown and overexpression on neointima formation, as well as on the proliferation, migration and phenotypic switching of VSMCs; and iii) to identify the downstream transcriptional targets of CDK9 that mediate these effects. The results of this study may expand the current understanding of neointimal hyperplasia and provide novel insights into the development of therapeutic strategies for restenosis.

Materials and methods

Materials. iCDK9 (cat. no. HY-16462), CDK9 degrader Thal-SNS-032 (Thal; cat. no. HY-123937), rapamycin (cat. no. HY-10219) and harmine (cat. no. HY-N0111) were obtained from MedChemExpress. Human platelet-derived growth factor-BB (PDGF-BB) protein (cat. no. 220-bb-010) was obtained from R&D Systems, Inc. Tamoxifen (cat. no. T5648) was purchased from Sigma-Aldrich (Merck KGaA). AAV2-SM22α-CDK9-overexpression ($7.13x10^{13}$ vg/ml) and AAV2-SM22α-negative control (NC) overexpression ($8.83x10^{13}$ vg/ml) vectors, both constructed with the same AAV2 backbone pAAV-SM22α-C-FH (cat. no. pAV100024-OE), were synthesized and purchased from Weizhen Biotechnology Co., Ltd.

Animals. All mice were housed in a specific pathogen-free laboratory under a 12-h light/dark cycle at 22-24˚C and 55±5% humidity, with free access to food and water. Male C57BL/6J mice (N000013) were purchased from GemPharmatech Co., Ltd. Mice were ~6 weeks old (body weight, 18-20 g) when subjected to AAV2 injection and 10 weeks old (body weight, 22-26 g) when subjected to carotid artery ligation. Before the surgical operation, mice were allocated to experimental groups using a computer-generated random number list. A total of 70 male C57BL/6J mice were used, in three cohorts: Sham, 2, 3 and 4 weeks after injury (7 mice/group); Sham, vehicle, iCDK9 5 and 10 mg/kg/day (7 mice/group); and AAV2-SM22α-NC and AAV2-SM22α-CDK9 (7 mice/group). Randomization was performed stratified by body weight to minimize baseline variation among the groups. Histological quantification of neointimal hyperplasia was performed by investigators blinded to group assignment, with tissue sections encoded with anonymous identifiers to achieve blinding. The intimal area, medial area and intima/media (I/M) ratio were measured with ImageJ software (version 1.54p; National Institutes of Health) by tracing the boundaries of the neointima (between the internal elastic lamina and the lumen) and the media (between the internal and external elastic laminae). Notably, surgeons could not be blinded due to the nature of the surgical procedures. Group sizes were estimated based on the effect size observed in our preliminary experiments and published study using the same carotid injury model, with α=0.05 and target power set to 0.8 (43). A formal a priori power calculation was not performed for the present study. Pre-specified exclusion criteria included peri-operative death, severe intraoperative bleeding and obvious surgical wound infection; animals meeting these criteria were to be excluded before statistical analysis and excluded animals would not be replaced. No animals met these criteria and no post hoc data exclusion was conducted. For western blotting semi-quantification, paired contralateral carotid vessels including right (non-ligated, RCA) and left (ligated, LCA) from the same mouse (n=3) were used to reduce inter-animal variation and technical bias during protein isolation, facilitating the detection of subtle flow-dependent protein changes. For systemic drug treatment and histological quantification of neointimal hyperplasia, independent mouse cohorts were adopted, since systemically delivered agents act on both carotid arteries within one animal and invalidate contralateral self-controls.

For iCDK9 treatment *in vivo*, 10-week-old male mice were subjected to carotid artery ligation, followed 3 days later by an 18-day iCDK9 (5 or 10 mg/kg/day) oral gavage regimen. After the last administration (scheduled endpoint), mice were euthanized by decapitation under 1.5% isoflurane anesthesia (induced with 3.0% isoflurane). The absence of breathing, heartbeat and corneal reflex was continuously observed for

>3 min to confirm complete death before tissue isolation, and the carotid arteries were then collected and subjected to subsequent experiments. For AAV2-mediated gene delivery, SMC-specific CDK9 overexpression was achieved using the aforementioned AAV2 vector, in which the transgene is driven by the SM22α promoter. Briefly, ~6-week-old male C57BL/6J mice were randomly divided into two groups and subjected to tail vein injection with equal doses of viral vectors; specifically, mice in the CDK9 overexpression group were injected with $5x10^{11}$ vg AAV2-SM22α-CDK9 overexpression virus, whereas mice in the NC group received $5x10^{11}$ vg AAV2-SM22α-NC overexpression virus. A total of 4 weeks after AAV2 virus transfection, three mice were randomly selected from each experimental group to verify the overexpression efficiency of CDK9 by western blot analysis and to confirm successful model construction. Subsequently, carotid artery ligation was performed on the remaining mice. All mice were sacrificed as aforementioned for sample collection 2 weeks after surgery, and the vascular tissues were harvested to detect and evaluate the degree of neointimal hyperplasia.

Mouse carotid artery ligation. Only male mice were used in the present study. For all surgical procedures, 10-week-old male mice were anesthetized with an intraperitoneal injection of sodium pentobarbital (50 mg/kg; Sigma-Aldrich; Merck KGaA). Subsequently, the left carotid artery (LCA) was carefully dissected and completely ligated at the proximal end of the carotid bifurcation with a 5-0 silk suture. A similar procedure without ligation on the right carotid artery (RCA) was used as a sham operation group. A total of 14, 21 or 28 days after surgery, carotid arteries were collected and subjected to subsequent experiments.

Immunofluorescence staining and immunohistochemistry (IHC). Mice were euthanized by decapitation after induction with 3.0% isoflurane and maintenance with 1.5% isoflurane. The carotid arteries were then perfused and embedded in optimal cutting temperature agent (cat. no. 4583; Sakura Finetek USA, Inc.), snap-frozen in liquid nitrogen and stored at -80˚C. Frozen sections were cut in a cryostat at -20˚C. Frozen sections (5 μm) and VSMCs grown on glass coverslips were fixed with 4% paraformaldehyde (PFA) for 10 min at room temperature, after being washed with PBS three times and permeabilized with 0.1% Triton X-100 in PBS for 5 min at room temperature. Cells and tissues were then blocked in 1% goat serum (cat. no. SL038; Beijing Solarbio Science & Technology Co., Ltd.) at room temperature and incubated with the following primary antibodies at 4˚C overnight: Anti-α-SMA (cat. no. BM0002; Wuhan Boster Biological Technology, Ltd.), anti-CDK9 (cat. no. ab239364; Abcam) anti-Pol II (cat. no. sc-55492; Santa Cruz Biotechnology, Inc.) and anti-p-Ser2 (cat. no. ab5095; Abcam). After incubation with Goat anti-Rabbit IgG (H+L) Cross-Adsorbed Secondary Antibody, Alexa Fluor™ 594 and Goat anti-Mouse IgG (H+L) Cross-Adsorbed Secondary Antibody, Alexa Fluor 647 secondary antibodies (cat. nos. A-11012 and A-21235; Invitrogen; Thermo Fisher Scientific, Inc.) for 1 h at room temperature, the nuclei were stained with DAPI (cat. no. P0131; Beyotime Biotechnology). Confocal immunofluorescence images were acquired with a confocal laser scanning microscopy (STELLARS 5; Leica Microsystems). Alexa Fluor 594-labelled signals (CDK9 and p-Ser2) were pseudo-coloured green and Alexa Fluor 647-labelled signals (α-SMA) were pseudo-coloured red for presentation; DAPI is shown in blue.

In addition, mouse carotid arteries were collected and fixed with 4% PFA for 24 h before embedding in paraffin at room temperature. Paraffin sections (5-μm thick) were prepared. Hematoxylin and eosin (H&E) staining and IHC for Ki67 were performed by Wuhan Servicebio Technology Co., Ltd. Paraffin sections were dewaxed in xylene substitute (cat. no. G1128; Wuhan Servicebio Technology Co., Ltd.) and rehydrated through graded ethanol (anhydrous ethanol twice, 75% ethanol, 5 min each). For H&E staining, sections were treated with pretreatment solution for 1 min, stained with hematoxylin for 3 min, differentiated for 3-5 sec, blued for 3-6 sec, dehydrated in 95% ethanol for 1 min and counterstained with eosin for 15 sec (H&E kit; cat. no. G1076; Wuhan Servicebio Technology Co., Ltd.). Sections were then dehydrated, cleared and mounted. For IHC, sections were subjected to antigen retrieval in citrate buffer (pH 6.0; cat. no. G1202; Wuhan Servicebio Technology Co., Ltd.) in an automated retrieval device (ARI-4; Wuhan Servicebio Technology Co., Ltd.), and endogenous peroxidase was blocked with 3% methanol-H_2O_2 for 25 min at room temperature in the dark. After blocking with 3% BSA (cat. no. GC305010; Wuhan Servicebio Technology Co., Ltd.) for 30 min at room temperature, sections were incubated with anti-Ki67 antibody (cat. no. GB111499; dilution 1:200; Wuhan Servicebio Technology Co., Ltd.) at 4˚C overnight and then with HRP-conjugated goat anti-rabbit polymer secondary antibody (ready-to-use; cat. no. G1302; Wuhan Servicebio Technology Co., Ltd.) for 50 min at room temperature. Signals were developed with DAB (cat. no. G1212; Wuhan Servicebio Technology Co., Ltd.), counterstained with hematoxylin (cat. no. G1004; Wuhan Servicebio Technology Co., Ltd.) for 3 min, dehydrated, cleared and mounted. All steps were performed at room temperature. Sections were examined by brightfield microscopy (SWE-CX63 and LG-S80; Wuhan Servicebio Technology Co., Ltd.) and images were analysed with Saiviewer software (Wuhan Servicebio Technology Co., Ltd.); scale bars are shown in each photomicrograph. Images were acquired with a Tissue FAX Plus microscope (brightfield; TissueGnostics GmbH). Morphometric analysis was performed using ImageJ software (version 1.54p; National Institutes of Health).

Cell culture and treatment. Human aortic VSMCs (HA-VSMCs; cat. no. HUM-iCell-c010) were purchased from iCell Bioscience, Inc. HA-VSMCs were cultured in primary SMC culture medium (cat. no. PriMed-iCell-004; iCell Bioscience, Inc.) in a humidified incubator at 37˚C with 5% CO_2. Primary rat VSMCs (rVSMCs) were isolated from the thoracic aorta of rats and routinely cultured in DMEM (cat. no. PM150210; Procell Life Science & Technology Co., Ltd.) supplemented with 10% fetal bovine serum (FBS; cat. no. FSP500; Shanghai ExCell Biology, Inc.) and 1% penicillin-streptomycin (cat. no. PB180120; Procell Life Science & Technology Co., Ltd). Briefly, two male Sprague-Dawley rats (3-4 weeks old; body weight 80-100 g; cat. no. D000017) were obtained from GemPharmatech Co., Ltd. Rats were housed under the same conditions as the mice and deeply anesthetized via an

intraperitoneal injection of sodium pentobarbital (50 mg/kg), and were then euthanized with an overdose of sodium pentobarbital (150 mg/kg). Death was confirmed as aforementioned for the mice. The adventitia and endothelium of fresh thoracic aorta vascular tissue were removed, and the medial layer was cut into small pieces and cultured in DMEM containing 20% FBS. Once VSMCs migrated out from the tissue explants, the medium was replaced with DMEM containing 10% FBS and 1% penicillin-streptomycin. The purity of VSMCs was identified by immunofluorescence with an antibody against a specific marker, namely α-SMA (1:500; cat. no. BM0002; Wuhan Boster Biological Technology, Ltd.), with overnight incubation at 4˚C. Both HA-VSMCs and rVSMCs were used in subsequent experiments between passages 2 and 4. Before treatment with the indicated agents, cells were starved with serum-free DMEM for 24 h. For the indicated experiments, VSMCs were treated at 37˚C for 24 h with PDGF-BB (20 ng/ml), iCDK9 (2 μM), Thal (2 μM) or rapamycin (50 nM). For harmine treatment, cells were incubated with harmine (10 or 20 μM) in complete medium at 37˚C for 24 h; control cells received an equal volume of DMSO (final concentration ≤0.1%).

Reverse transcription-quantitative PCR (RT-qPCR). Total RNA was isolated from cultured VSMCs using TRIzol® reagent (cat. no. YZ-15596018; Invitrogen; Thermo Fisher Scientific, Inc.) following the manufacturer's protocol. The extracted RNA was reverse transcribed using the Hifair® II 1st Strand cDNA Synthesis kit (cat no. 11123ES60; Shanghai Yeasen Biotechnology Co., Ltd.) to obtain cDNA. qPCR was then performed using a qPCR kit (cat. no. 11204ES08; Shanghai Yeasen Biotechnology Co., Ltd.), with the primer sequences listed in Table SI. All experiments were conducted in triplicate. The thermocycling conditions were set as follows: Initial denaturation at 95˚C for 3 min, followed by 40 cycles at 95˚C for 10 sec and 60˚C for 30 sec, with melting curve analysis for product specificity verification. Relative target gene expression was calculated using the $2^{-\Delta\Delta Cq}$ quantification method (44), and all data were normalized to the housekeeping gene GAPDH.

Cell proliferation assay. The 5-ethynyl-2'-deoxyuridine (EdU) incorporation assay (cat. no. C0078S; Beyotime Biotechnology) was performed to assess VSMC proliferation according to the manufacturer's instructions. Briefly, after treatment, the VSMCs (seeded in 12-well plates at $5x10^4$ cells/well) were incubated with EdU at a final concentration of 10 μM for 4 h at 37˚C before measurement, and total cellular nuclei were stained with Hoechst 33342 (1:1,000; cat. no. C0078S; Beyotime Biotechnology) at room temperature for 10 min. EdU-positive cells were captured with an EVOS FL Auto2 fluorescence microscope (Invitrogen; Thermo Fisher Scientific, Inc.) and measured using ImageJ software.

In vitro migration assay. A wound-healing assay was used to measure the migratory ability of VSMCs. Briefly, after serum starvation for 12 h, VSMCs cultured in 12-well plates (~90% confluence) were scratched with sterile plastic 10-μl micro-pipette tips to draw a straight line in the middle of the wells, and were washed twice with 1X PBS to remove cellular debris. Subsequently, VSMCs were treated with the indicated agents for an additional 24 h, and images were acquired with an EVOS FL Auto2 brightfield microscope. The migration area was analyzed using ImageJ software.

Recombinant adenovirus construction and transfection. CDK9-overexpressing recombinant adenovirus (Adv-CDK9) and blank control recombinant adenovirus (Adv-Ctrl) were purchased from Weizhen Biotechnology Co., Ltd. Human CDK9 cDNA was packaged into the adenoviral vector pADM-CMV-mCMV-copGFP, and an empty vector was used as a control (Adv-Ctrl). HA-VSMCs at 50-60% confluence were infected with the adenoviruses (multiplicity of infection, 10 or 20) at 37˚C for 24 h and the medium was then replaced with fresh primary SMC culture medium. After incubation for 24 h, cells were harvested for subsequent experiments.

Western blot analysis. After treatment, cultured cells were harvested and lysed in RIPA buffer (cat. no. P0013B; Beyotime Biotechnology) with complete protease inhibitors (cat. no. 05892791001; Roche Applied Science) and phosphatase inhibitors (cat. no. 4906837001; Roche Applied Science), and the supernatant was obtained through centrifugation at 13,800 x g for 10 min at 4˚C. After determining the protein concentration with a BCA Protein Assay Kit (cat. no. A55864; Thermo Fisher Scientific, Inc.), equal amounts of protein (20 μg) were separated by SDS-PAGE. Briefly, 8% gels were used for high-molecular-weight proteins, whereas 12% gels were applied for the detection of low-molecular-weight proteins such as Twist1 (~26 kDa). For tissue extraction, mouse aorta tissues were excised and homogenized in RIPA buffer; the supernatant was then collected and processed for subsequent experiments in the same manner as cultured cells. The proteins were transferred to a 0.22-μm PVDF membrane at 240 mA for 90 min and the membranes were blocked with 5% non-fat milk at room temperature for 2 h. Subsequently, the membranes were incubated with primary antibodies against the indicated proteins at 4˚C overnight, followed by incubation with secondary antibodies at room temperature for 1 h. Antibody details are listed in Table SII. Semi-quantification of western blotting bands, which were visualized by enhanced chemiluminescence (cat. no. K-12045-D50; Advansta Inc.), was performed using ImageJ software.

Small interfering RNA (siRNA) transfection. siRNAs targeting human CDK9, human Twist1 and siRNA NC were synthesized by Shanghai GenePharma Co., Ltd. The siRNA sequences are provided in Table SIII. VSMCs at 30-50% confluence were pre-incubated in transfection medium (Opti-MEM; cat. no. 31985070; Gibco; Thermo Fisher Scientific, Inc.) and were then transfected with siRNAs (50 nM) using Lipofectamine® RNAi MAX (cat. no. 13778150; Invitrogen; Thermo Fisher Scientific, Inc.) according to the manufacturer's instructions. A total of 6 h post-transfection 37˚C, the medium was replaced with fresh serum-free DMEM, and the cells were cultured for another 18 h before being subjected to the subsequent experiments.

Dual luciferase assay. For the luciferase reporter assay, the promoter region of the Twist1 gene (from -2,000 to +200 bp relative to the transcription start site) was cloned into the pGL3-Basic vector (cat. no. E1751; Promega Corporation) to

generate the Twist1-promoter reporter plasmid. Human 293T cells (cat. no. CL-0005; Procell Life Science & Technology Co., Ltd.) were cultured in DMEM (cat. no. PM150210; Procell Life Science & Technology Co., Ltd.) supplemented with 10% FBS at 37˚C in 5% CO_2 and seeded in 12-well plates at 70-80% confluence. Cells were co-transfected with 100 ng pGL3-Basic or Twist1-promoter plasmid, combined with 300 ng empty PRK5M vector or PRK5M-CDK9 overexpression plasmid (kindly provided by Professor Yuhua Xue, School of Pharmaceutical Sciences, Xiamen University, Xiamen, China) using Lipofectamine® 3000 (cat. no. L3000015; Invitrogen; Thermo Fisher Scientific, Inc.). Meanwhile, 20 ng pRL-SV40 *Renilla* luciferase plasmid (cat. no. E2261; Promega Corp.) was co-transfected into all groups to normalize transfection efficiency. A total of 48 h post-transfection, cellular luciferase activity was detected using a Dual Luciferase Reporter Gene Assay Kit (cat. no. RG027; Beyotime Biotechnology) in strict accordance with the manufacturer's instructions. The luciferase signal was detected using a microplate reader (SpectraMax iD3; Molecular Devices, LLC), and the relative luciferase activity was calculated as the ratio of firefly luciferase signal to *Renilla* luciferase signal with the pGL3-empty vector group set as the control for comparison.

Chromatin immunoprecipitation (ChIP)-qPCR assay. The ChIP-qPCR assay was performed as described previously with minor modifications (45). Briefly, after treatment with PDGF-BB (20 ng/ml) or control agent (PBS with 0.1% BSA) for 24 h, rVSMCs were fixed with 1% (wt/vol) formaldehyde (10 min) and subsequently quenched with glycine (1.25 M, 5 min) at room temperature. After washing with PBS twice, the cells were resuspended in lysis buffer (50 mM Tris-HCl pH 8.0, 10 mM EDTA, 1% SDS) containing a protease inhibitor cocktail before sonication (5 sec on and 10 sec off for a total of 30 cycles) to obtain chromatin fragments of 100-500 bp. IP was carried out overnight at 4˚C with 3 μg anti-CDK9 antibody (cat. no. ab239364; Abcam) or 3 μg normal rabbit IgG (cat. no. 2729S; CST Biological Reagents Co., Ltd.) as a NC. Protein A/G agarose beads (20 μl per sample; cat. no. 20421; Thermo Fisher Scientific, Inc.) was used to pull down the antigen-antibody compounds, then washed three times with low salt buffer [0.1% SDS, 1% Triton X-100, 2 mM EDTA, 20 mM Tris-HCl (pH 8.0), 150 mM NaCl] and one time with LiCl immune complex wash buffer [0.25 M LiCl, 1% IGEPAL CA-630, 1% deoxycholic acid, 1 mM EDTA, 10 mM Tris (pH 8.0)]. After the cross-linking was reversed at 65˚C overnight, chromatin fragments were treated with RNase A (cat. no. R6513; 100 μg/ml; Sigma-Aldrich; Merck KGaA) and proteinase K (cat. no. P2308; 50 μg/ml; Sigma-Aldrich; Merck KGaA) at 55˚C for 1 h. DNA from each sample was purified using the QIAquick PCR Purification Kit (cat. no. 28104; Qiagen, Inc.) and the occupancy of CDK9 on the Twist1 gene promoter was determined by qPCR as aforementioned with the primers listed in Table SIV.

Transcriptomic profiling. To determine the potential target of CDK9 in regulating VSMC phenotypic switching, rVSMCs were treated with DMSO (0.1%, as a control), the phenotypic switching activator PDGF-BB (20 ng/ml), the inhibitor rapamycin (50 nM) or iCDK9 (2 μM) for 24 h at 37˚C. Total RNA was extracted from VSMCs using TRIzol reagent, according to the manufacturer's instructions. RNA integrity was assessed with an Agilent 5300 Bioanalyzer (Agilent Technologies, Inc.) and analyzed for concentration and purity using a NanoDrop 2000 instrument (NanoDrop Technologies; Thermo Fisher Scientific, Inc.). RNA purification, reverse transcription, library construction and sequencing were performed by Shanghai Majorbio Bio-pharm Technology Co., Ltd., according to the manufacturer's instructions (Illumina, Inc.). RNA-seq libraries were prepared with the Illumina® Stranded mRNA Prep, Ligation kit (cat. no. 20040534; Illumina, Inc.) from 1 μg of total RNA: mRNA was enriched with oligo(dT) beads and fragmented, double-stranded cDNA was synthesized with random hexamer primers, with dUTP incorporation enabling strand-specific retention of first-strand cDNA, and the cDNA was then subjected to end repair, phosphorylation, 'A' base addition and adapter ligation, followed by size selection for 300-bp fragments and 15 cycles of PCR amplification. RNA-seq was carried out on a NovaSeq X Plus (Illumina, Inc.) in paired-end mode (2x150 bp) using the NovaSeq X Series 25B Reagent Kit (300 cycles; cat. no. 20104706; Illumina, Inc.), with a loading concentration of 1.5 pM. Raw paired-end reads were quality-controlled using fastp (v0.23.2; https://github.com/OpenGene/fastp) with default parameters, and clean reads were aligned to the reference *Rattus norvegicus* genome mRatBN7.2 (https://asia.ensembl.org/Rattus_norvegicus/Info/Index) using HISAT2 (v2.2.1; http://ccb.jhu.edu/software/hisat2/index.shtml). Transcript abundances were quantified with RSEM (v1.3.3; https://deweylab.github.io/RSEM/) and expressed as TPM. To identify the significantly differentially expressed genes (DEGs), the expression level of each transcript was calculated according to the transcripts per million reads method. RNA-Seq by Expectation-Maximization was used to quantify gene abundances. DEGs with a fold-change ≥2 and $P<0.05$ were considered significant DEGs. Furthermore, Gene Ontology analysis was performed using GOATOOLS (version v0.8.4; https://github.com/tanghaibao/GOatools) using Fisher's exact test with Bonferroni correction.

Statistical analysis. Statistical analyses were performed to assess the significance of the differences observed in the experiments. All *in vitro* experiments were independently repeated three times (n=3). All data are presented as the mean ± SEM and were analyzed using GraphPad Prism 10 (GraphPad; Dotmatics). Comparisons between two groups were made using paired or unpaired Student's t-tests as appropriate. One-way ANOVA followed by Tukey's post hoc test was used when a single independent variable was compared among more than two groups, and two-way ANOVA followed by Tukey's multiple comparison test was used when two independent variables were present. When Levene's test indicated unequal variances among the groups, the data were log10-transformed prior to one-way ANOVA, and Tukey's post hoc test was applied to the transformed values. $P<0.05$ was considered to indicate a statistically significant difference.

Results

CDK9 expression and activity are induced in VSMCs during neointimal hyperplasia. To investigate the role of CDK9 in neointimal formation, a mouse carotid artery injury model was

established through ligation initially, and neointimal formation gradually increased >2 weeks after injury (Fig. 1A). Notably, after carotid artery ligation in mice, CDK9 expression was induced in a time-dependent manner in response to the injury, which was accompanied by a notable decrease in the contractile VSMC marker α-SMA (Fig. 1B and C). Additionally, as a surrogate marker for CDK9-dependent transcriptional activity, the p-Ser2 level of RNA Pol II was significantly increased after injury (Fig. 1D and E), whereas immunofluorescence staining showed no significant change in total RNA Pol II intensity at the same time points (Fig. S1A and B). Furthermore, western blot analysis confirmed the significant increase in CDK9 and p-Ser2 expression levels at the sites of injury 28 days after ligation compared with in the non-ligated vessels (Fig. 1F and G).

As shown in Fig. 1B, CDK9 was largely co-localized with α-SMA-positive VSMCs. To determine whether the increase in CDK9 expression and p-Ser2 level was due to the phenotypic modulation of VSMCs in the process of injury-induced neointimal formation, HA-VSMCs were treated with PDGF-BB (20 ng/ml) and rapamycin (50 nM). As expected, α-SMA expression was decreased after PDGF-BB treatment, but increased in the rapamycin group, whereas both the mRNA and protein levels of CDK9 were markedly elevated after PDGF-BB treatment, and rapamycin inhibited CDK9 expression (Fig. 1H-J). Meanwhile, the change in p-Ser2 level was consistent with that of CDK9 (Fig. 1I and J). In addition, the level of KLF4, a transcription factor that drives the synthetic phenotype of VSMCs, was increased by PDGF-BB and decreased by rapamycin, similar to the change in p-Ser2 (Fig. 1I and J). Similar results were observed in rVSMCs (Fig. S2). Taken together, these data indicate that CDK9 is involved in neointimal formation after vascular injury and VSMCs phenotypic switching.

Inhibition of CDK9 alleviates neointimal formation following vascular injury. To confirm the role of CDK9 in neointimal formation, a specific iCDK9 was employed in the present vascular injury model. As shown in Fig. 2A, ~10-week-old mice were subjected to ligation of the LCA, and 3 days post-surgery, iCDK9 (5 or 10 mg/kg) was administered via oral gavage daily. The H&E staining results showed that, 3 weeks after ligation, intimal hyperplasia was obvious, and this could be alleviated by iCDK9 treatment in a dose-dependent manner with a significant decrease in the intimal area and a lower intima/media ratio (Fig. 2B and C).

Furthermore, immunofluorescence staining of the contractile VSMC marker α-SMA showed that the decrease in α-SMA expression after vascular injury could be suppressed by iCDK9 treatment (Fig. 2D and E). In addition, the p-Ser2 level in the ligated carotid artery was markedly decreased after iCDK9 treatment (Fig. 2F and G), whereas immunofluorescence staining showed no significant change in total RNA Pol II intensity (Fig. S3A and B). Taken together, these data suggested that iCDK9 can relieve neointimal hyperplasia after vascular injury in a kinase activity-dependent manner.

To further clarify the regulatory role of CDK9 in vascular neointimal hyperplasia, an AAV2 vector driven by the SM22α promoter was utilized to achieve specific overexpression of CDK9 in SMCs (Fig. S4A). It was revealed that SMC-specific CDK9 overexpression exerted no marked effect on vascular morphology in uninjured blood vessels (Fig. S4B and C). However, CDK9 overexpression significantly exacerbated neointimal hyperplasia induced by vascular injury (Fig. 2H and I). Thus, consistent with the pharmacological inhibition results, genetic overexpression of CDK9 in SMCs further validated the pro-hyperplastic function of CDK9 in injured vessels. Collectively, these loss- and gain-of-function experiments demonstrated that CDK9 acts as a critical positive regulator of vascular injury-induced neointimal hyperplasia.

CDK9 regulates the proliferation and migration of VSMCs. As VSMC proliferation and migration are key processes in neointimal formation following arterial injury (19), the present study next aimed to determine whether the effects of CDK9 on neointimal formation were due to the regulation of VSMC proliferation and migration. First, the potential role of CDK9 in PDGF-BB-induced cell migration and proliferation were examined *in vitro* models. To evaluate the effect of CDK9 on HA-VSMC migration, a wound-healing assay was performed. It is known that the motility of VSMCs can be promoted by PDGF-BB stimulation (43). The results revealed that iCDK9 (2 μM) or the selective CDK9 degrader Thal (2 μM) significantly restricted the wound closure under both quiescent and PDGF-BB-stimulated conditions (Fig. 3A and B).

VSMC proliferation is another key mechanism in the process of neointimal formation. Next, the regulatory effect of CDK9 on VSMC proliferation was evaluated in the present study. To this end, PDGF-BB-stimulated VSMCs were subjected to EdU incorporation assays. After PDGF-BB (20 ng/ml) stimulation, the number of EdU-positive cells was markedly increased; however, this could be inhibited by iCDK9 or the degrader Thal (Fig. 3C and D). To further verify the regulatory effect of CDK9 on the proliferation of VSMCs, CDK9 was knocked down in VSMCs by siRNA, knockdown efficiency was confirmed by western blotting (Fig. S5E). The results showed that, after CDK9 knockdown, the protein expression levels of the cell proliferation marker proliferating cell nuclear antigen (PCNA) were significantly decreased (Fig. 3E and F). However, when CDK9 was overexpressed by adenovirus infection, the protein expression levels of PCNA were markedly increased in VSMCs (Fig. 3G and H). VSMC proliferation was further evaluated *in vivo*, with another cell proliferation marker, Ki67, investigated by IHC. The expression levels of Ki67 were higher in LCAs after 3 weeks of ligation than in the non-ligated RCAs (sham); however, inhibition of CDK9 activity by iCDK9 markedly suppressed Ki67 expression levels in the LCA compared with that in the sham group (Fig. 3I). Taken together, these results indicated that inhibition or deficiency of CDK9 in VSMCs can suppress their migration and proliferation, thereby alleviating injury-induced neointimal formation.

Inhibition of CDK9 can suppress the phenotypic switching of VSMCs in vitro. Phenotypic switching of VSMCs, from the differentiated contractile to the dedifferentiated synthetic state, serves an important role in neointimal formation after vascular injury. Consistent with the inhibitory effect of iCDK9 on neointimal formation *in vivo*, iCDK9 (2 μM) upregulated the basal levels of the VSMC contractile marker α-SMA,

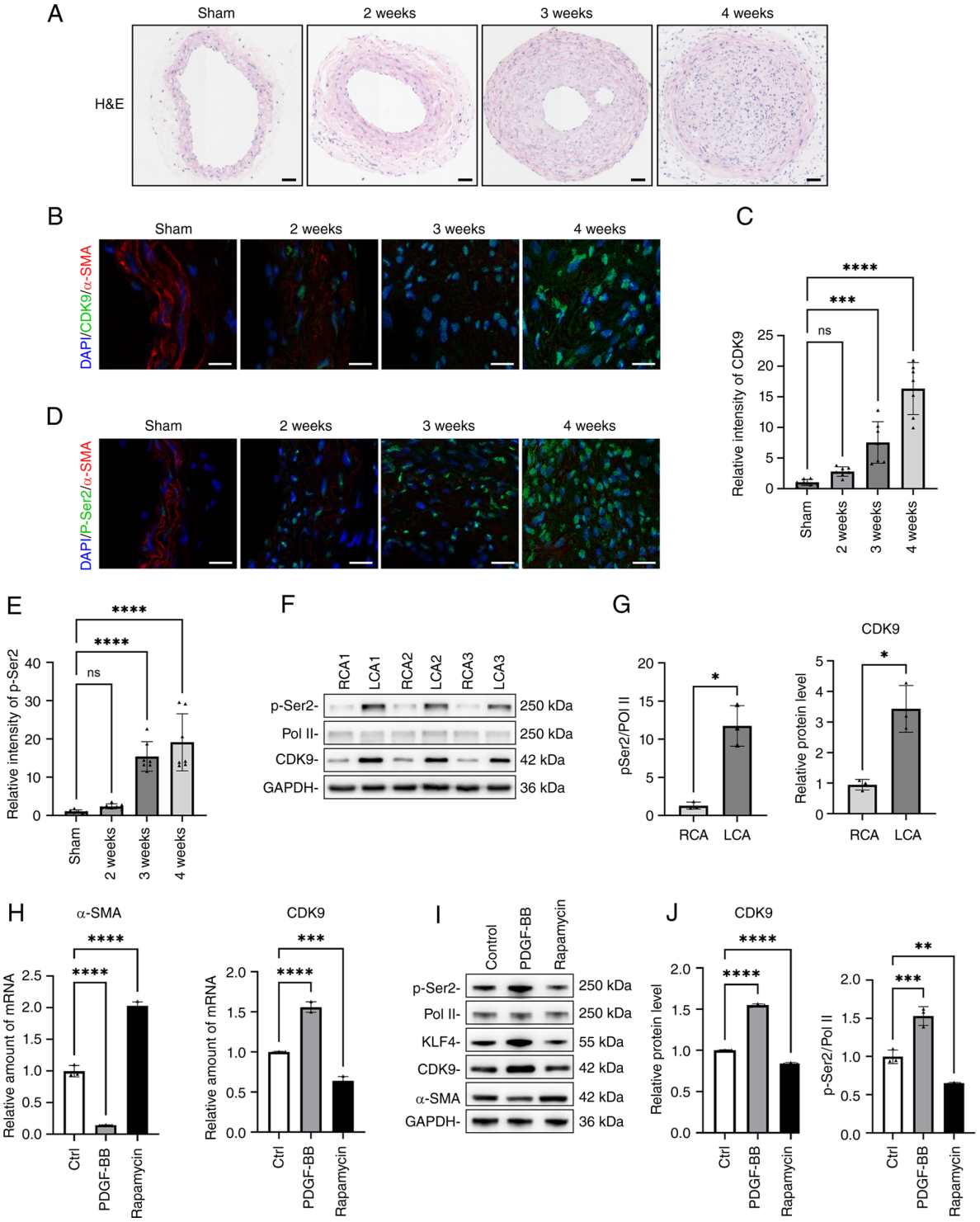


Figure 1. Expression and activity of CDK9 are induced in VSMCs during neointimal hyperplasia. (A) C57BL/6J mice were subjected to carotid artery ligation, and representative images of H&E-stained carotid arteries were obtained at 2, 3 and 4 weeks post-injury. Scale bar, 50 μm; n=7 animals/group. (B) Representative images of immunofluorescence staining of CDK9 and α-SMA in the carotid arteries at the indicated time after injury. Scale bar, 50 μm; n=7 animals/group. (C) Quantitative analysis of relative CDK9 intensity. (D) Representative images of immunofluorescence staining of p-Ser2 and α-SMA in the carotid arteries at the indicated times after injury. Scale bar, 50 μm; n=6 animals/group. (E) Quantitative analysis of relative p-Ser2 intensity. (F) Western blot analysis of p-Ser2 and CDK9 levels in the RCAs (control) and LCAs of C57BL/6J mice at 4 weeks post-injury. (G) Semi-quantification of p-Ser2 and CDK9 levels. p-Ser2 was normalized to total Pol II. The protein expression levels were normalized to GAPDH. n=3 animals/group. CDK9 activity was assessed using p-Ser2, the direct product of CDK9 kinase activity, normalized to total Pol II. (H) Quantitative PCR analysis was performed to detect the mRNA levels of CDK9 and α-SMA in HA-VSMCs after treatment with PDGF-BB or rapamycin for 24 h. Three biological replicates were analyzed. (I) Western blot analysis of p-Ser2, Pol II, KLF4, CDK9 and α-SMA in VSMCs after treatment with PDGF-BB or rapamycin for 24 h. Three biological replicates were analyzed and representative blots from three independent experiments are shown. (J) Semi-quantification of the indicated protein levels. Protein expression levels were normalized to GAPDH. Data are presented as the mean ± SEM. *P<0.05, **P<0.01, ***P<0.001 and ****P<0.0001. Statistical significance was assessed by one-way ANOVA followed by Tukey's post hoc test or unpaired Student's t-test or a paired Student's t-test (for the RCAs and LCAs from the same animals, Fig. 1G). All data are from biological replicates. α-SMA, α-smooth muscle actin; CDK9, cyclin-dependent kinase 9; H&E, hematoxylin and eosin; KLF4, Krüppel-like factor 4; LCA, left carotid artery; ns, not significant; p-Ser2, phosphorylated RNA polymerase II (Ser2); PDGF-BB, platelet-derived growth factor-BB; Pol II, RNA polymerase II; RCA, right carotid artery; HA-VSMC, human aortic vascular smooth muscle cell.

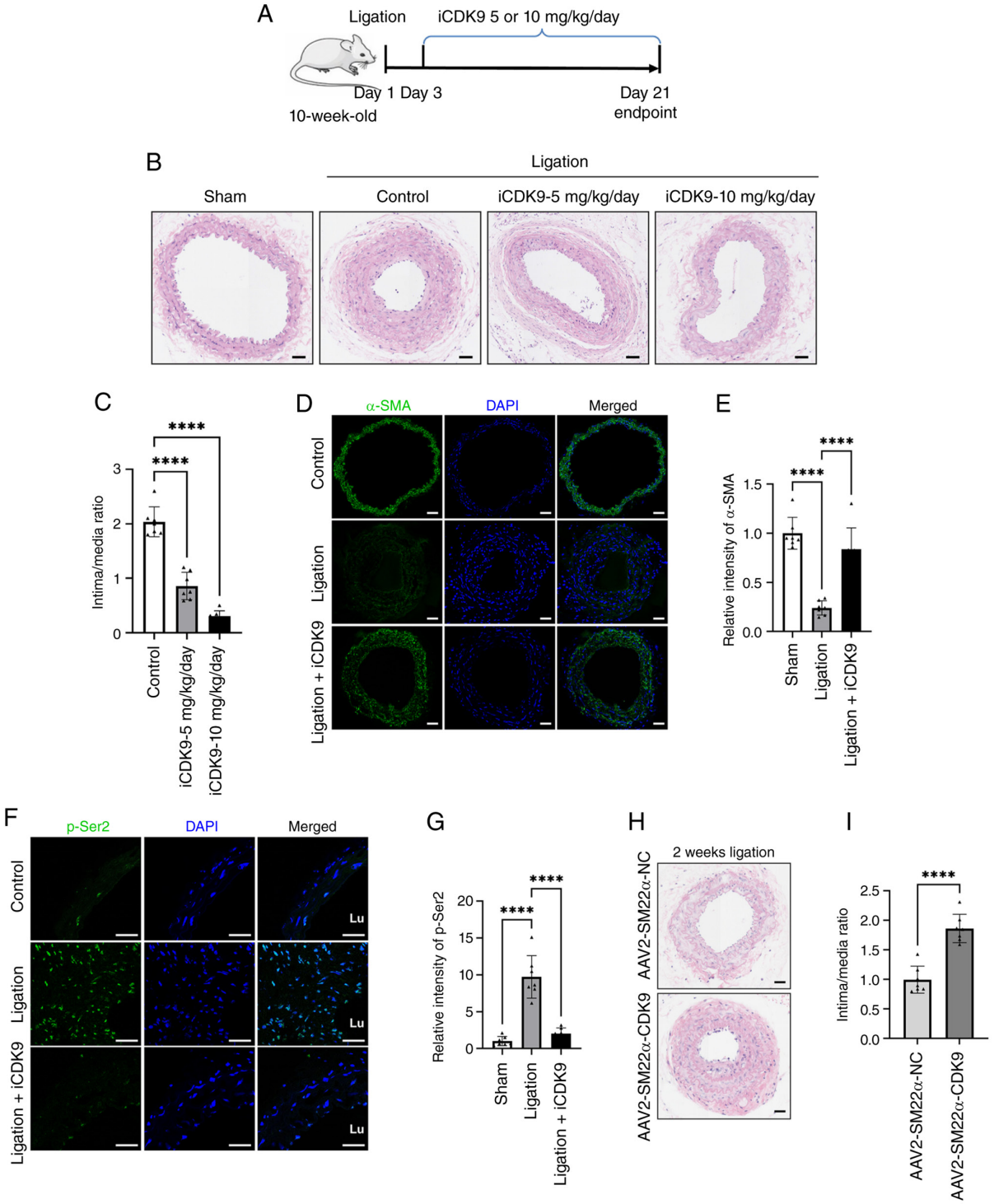


Figure 2. iCDK9 suppresses neointima formation following vascular injury. (A) Schematic workflow for iCDK9 treatment *in vivo*. (B) Representative images of H&E-stained carotid arteries of mice 21 days after injury in the vehicle control or iCDK9 treatment groups. Scale bar, 50 μm, n=7 animals/group. (C) Quantification analysis of the intima/media ratio. (D) Carotid arteries on day 21 post-injury with or without iCDK9 treatment were subjected to immunofluorescence to evaluate the contractile marker α-SMA. Scale bar, 50 μm; n=5 animals/group. (E) Quantification of the relative intensity of α-SMA. (F) Representative immunofluorescence staining of the relative intensity of p-Ser2 in carotid arteries on day 21 post-injury with or without iCDK9 treatment. Scale bar, 50 μm; n=7 animals/group. (G) Quantification of relative intensity of p-Ser2. Scale bar, 50 μm; n=7 animals/group. (H) Representative images of H&E-stained carotid arteries of mice 2 weeks after injury in the AAV2-SM22α-NC or AAV2-SM22α-CDK9 groups. (I) Quantification analysis of the intima/media ratio. Data are presented as the mean ± SEM. ****P<0.0001. Statistical significance was assessed by one-way ANOVA with Tukey's post hoc test or unpaired Student's t-test. All data are from biological replicates. α-SMA, α-smooth muscle actin; CDK9, cyclin-dependent kinase 9; H&E, hematoxylin and eosin; iCDK9, CDK9 inhibitor; NC, negative control; p-Ser2, phosphorylated RNA polymerase II (Ser2); SM22α, transgelin.

and downregulated the VSMC synthetic marker osteopontin (OPN) and the proliferation marker PCNA in VSMCs (Fig. 4A). In addition, p-Ser2 was decreased by iCDK9 in a concentration-dependent manner (Fig. S5A). Similar results were observed when the CDK9 selective degrader Thal was employed in VSMCs. Accompanied by decreases in both CDK9

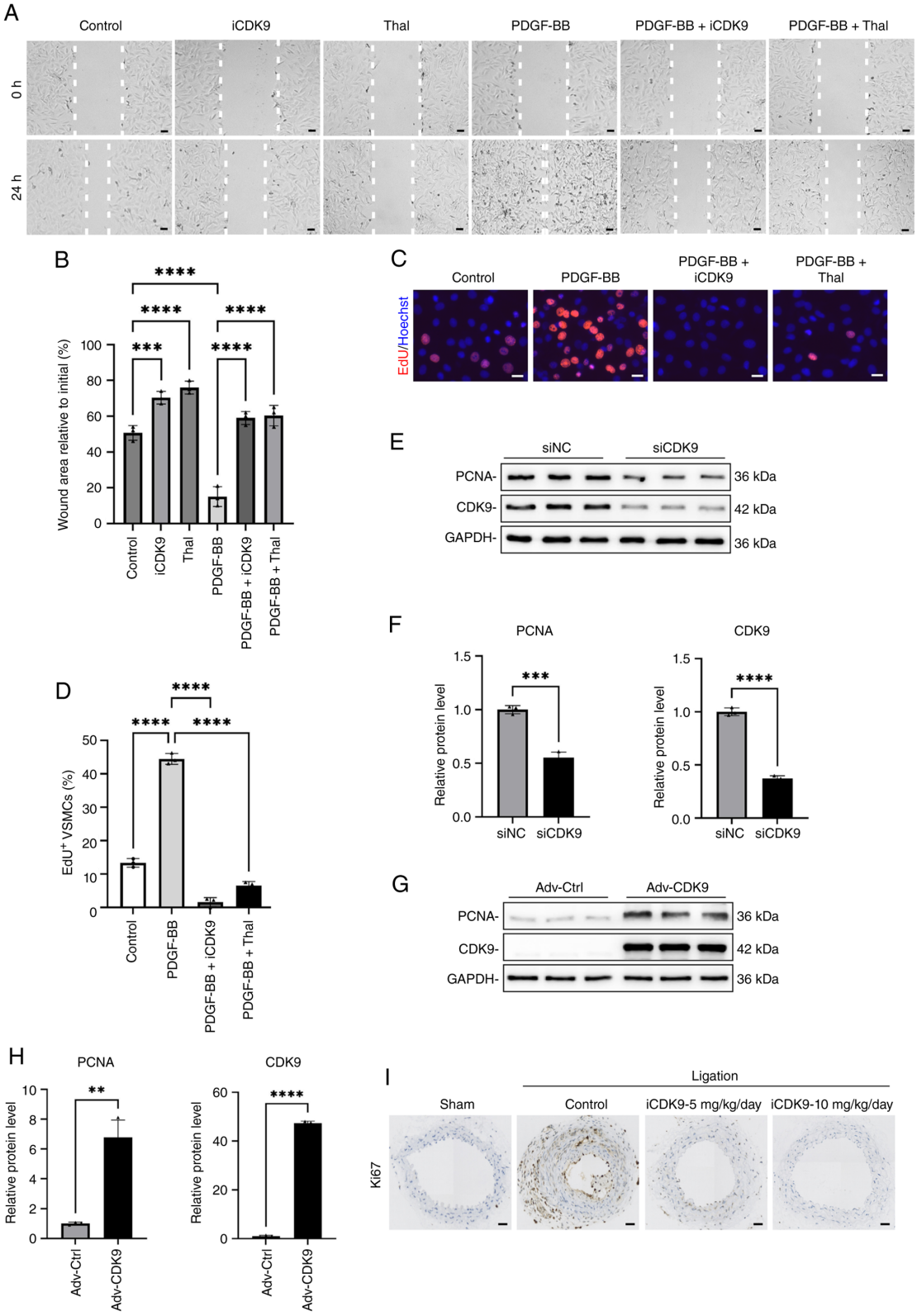


Figure 3. CDK9 regulates the proliferation and migration of smooth muscle cells. (A) Representative images of wound-healing assay in VSMCs. Scale bar, 20 μm. Three biological replicates were analyzed. (B) Quantification of the wound area relative to the initial area (%) at 24 h by ImageJ. (C) VSMCs were subjected to EdU incorporation assay and representative images are presented. Scale bar, 20 μm. Three biological replicates were analyzed. (D) Quantification of EdU-positive cells, as measured by ImageJ software. (E) Western blot analysis of PCNA and CDK9 protein expression levels in VSMCs transfected with siNC or siCDK9. Three biological replicates were analyzed and representative images are shown. (F) Semi-quantification of PCNA and CDK9 protein levels. The protein expression levels were normalized to GAPDH. (G) Western blot analysis of PCNA and CDK9 protein expression levels in VSMCs 48 h after infection with Adv-Ctrl or Adv-CDK9. Three biological replicates were analyzed and representative images are shown. (H) Semi-quantification of the indicated protein levels. The protein expression levels were normalized to GAPDH. (I) Representative cross-sections of immunohistochemically stained Ki67 (brown) in carotid arteries 21 days after injury with or without iCDK9 treatment. Scale bar, 50 μm; n=6 animals/group. Data are presented as the mean ± SEM. **P<0.01, ***P<0.001 and ****P<0.0001. Statistical significance was assessed by one-way ANOVA followed by Tukey's post hoc test or unpaired Student's t-test. All data are from biological replicates. Adv, adenovirus; CDK9, cyclin-dependent kinase 9; EdU, 5-ethynyl-2'-deoxyuridine; iCDK9, CDK9 inhibitor; NC, negative control; PCNA, proliferating cell nuclear antigen; PDGF-BB, platelet-derived growth factor-BB; si, small interfering; Thal, Thal-SNS-032; VSMC, vascular smooth muscle cell.

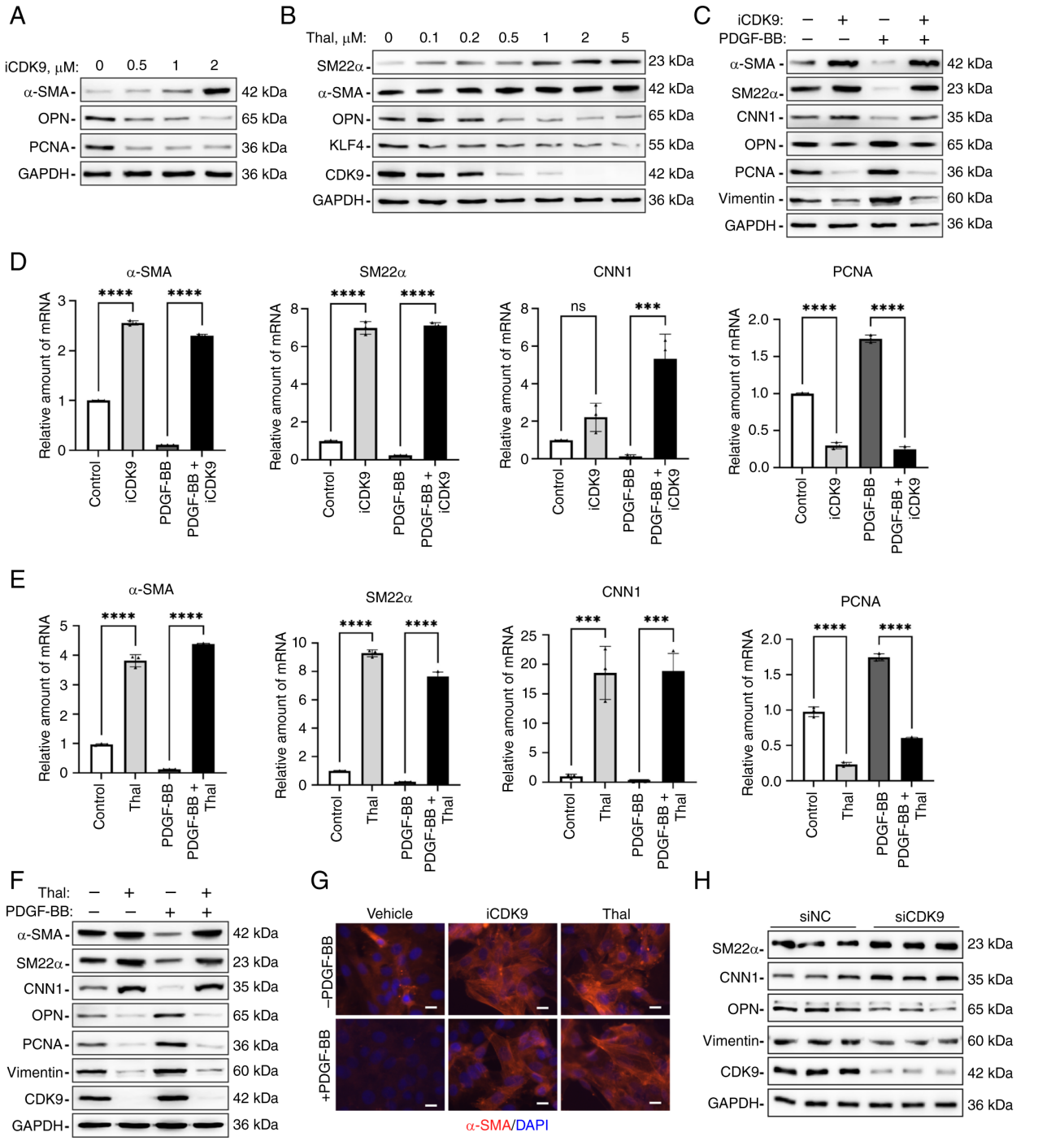


Figure 4. CDK9 inhibition in VSMCs results in an increase in the contractile phenotype. (A) Western blot analysis of the indicated proteins in VSMCs treated with iCDK9 at different concentrations for 24 h. (B) Western blot analysis of the indicated proteins in VSMCs treated with the CDK9 degrader Thal at different concentrations for 24 h. (C) VSMCs were treated with PDGF-BB in the presence or absence of iCDK9 for 24 h, and then subjected to western blot analysis to detect contractile and synthetic markers. After treatment with PDGF-BB (D) with or without iCDK9 for 24 h, and (E) with or without Thal for 24 h, the indicated mRNA levels in VSMCs were measured by reverse transcription-quantitative PCR. (F) Contractile and synthetic markers were detected by western blot analysis after VSMCs were treated with PDGF-BB in the presence or absence of Thal for 24 h. (G) Representative immunofluorescence staining of α-SMA in VSMCs after treatment with PDGF-BB in the presence of iCDK9 or Thal. Scale bar, 10 μm. (H) Western blot analysis of SM22α, CNN1, OPN, vimentin and CDK9 protein expression levels in VSMCs transfected with siNC or siCDK9 for 48 h. Data are presented as the mean ± SEM, ***P<0.001 and ****P<0.0001. Statistical significance was assessed by one-way ANOVA followed by Tukey's post hoc test. All data are from three biological replicates. α-SMA, α-smooth muscle actin; CDK9, cyclin-dependent kinase 9; CNN1, calponin 1; iCDK9, CDK9 inhibitor; KLF4, Krüppel-like factor 4; NC, negative control; OPN, osteopontin; PCNA, proliferating cell nuclear antigen; PDGF-BB, platelet-derived growth factor-BB; si, small interfering; SM22α, transgelin; Thal, Thal-SNS-032; VSMC, vascular smooth muscle cell.

protein and p-Ser2 levels after Thal (2 μM) treatment, the levels of contractile markers (α-SMA and SM22α) increased, but synthetic marker (OPN and KLF4) notably decreased (Figs. 4B and S5B). As an important dedifferentiation factor, PDGF-BB can stimulate VSMCs to undergo phenotypic switching, which is manifested as a decrease in differentiation marker genes, such as α-SMA and SM22α, and an increase in synthetic markers such as OPN (43). As expected, PDGF-BB

(20 ng/ml) markedly increased the levels of the cell proliferation marker PCNA and synthetic markers OPN and vimentin, but decreased the levels of contractile markers α-SMA, SM22α and CNN1; however, these changes were attenuated by iCDK9 (Fig. 4C and D). The PDGF-BB-induced increase in p-Ser2 was reversed by iCDK9 (Fig. S5C). Additionally, the CDK9 degrader Thal notably inhibited the changes in the expression of proteins related to VSMC phenotypic switching induced by PDGF-BB (Fig. 4E and F). Consistently, the PDGF-BB-induced increase in p-Ser2 was reversed by Thal (Fig. S5D). In addition, immunofluorescence assays further demonstrated that iCDK9 or Thal markedly increased the basal expression levels of α-SMA and inhibited PDGF-BB-induced VSMC phenotypic switching (Fig. 4G). These results were confirmed by RNA interference-mediated CDK9 knockdown experiments in HA-VSMCs. The levels of contractile phenotype-related proteins, such as SM22α and CNN1 were increased, whereas those of synthetic markers, such as vimentin and OPN were decreased in CDK9 siRNA-transfected HA-VSMCs (Figs. 4H and S5E). Taken together, these data suggested that CDK9 may have an important role in mediating the phenotypic switching of VSMCs, and inhibiting CDK9 could effectively inhibit phenotypic switching; thus, CDK9 may serve as a potential target for neointimal formation *in vivo*.

CDK9 regulates the expression level of Twist1. The present study next explored the underlying mechanisms of CDK9 in the phenotypic modulation of VSMCs. Since it has been reported that the process of VSMC phenotypic switching from the contractile to the synthetic state can be induced by PDGF-BB and suppressed by rapamycin (16,21), VSMCs were treated with PDGF-BB, rapamycin or iCDK9. Subsequently, whole transcriptome analysis was performed using RNA-seq. In total, 367 genes that were synchronously significantly altered under the various treatment conditions were selected for further analysis (Fig. 5A). The aforementioned results (Figs. 1-4) indicated that iCDK9 can inhibit the phenotypic switching of VSMCs as rapamycin does; thus, genes that exhibited consistent change trends in both the iCDK9 and rapamycin groups, yet showed opposite trends to the PDGF-BB group, were considered potential candidates for further research. Cluster analysis of these 367 genes showed that only 96 genes were significantly increased in the PDGF-BB group, whereas they were decreased in both the iCDK9 and rapamycin groups (Fig. 5B). As a key component of the P-TEFb complex, CDK9 mainly regulates the transcription process of intracellular genes (32); thus, the present study focused on the changes of transcription-related proteins. Gene Ontology analysis of the 96 selected genes revealed that four of them were transcription-related genes, including Twist1, Helz2, Jun and Mef2c (Fig. 5C).

As an important transcription factor, Twist1 regulates multiple biological processes, including epithelial-mesenchymal transition, cell proliferation, migration and ECM remodeling (46-48). Previous studies have reported that Twist1 can induce VSMC proliferation and phenotypic switching (49-51). Therefore, it was speculated whether CDK9 may promote the phenotypic switching of smooth muscle by regulating the expression of Twist1. To this end, the RNA-seq results were first validated using RT-qPCR and it was found that, consistent with the sequencing results, the mRNA levels of Twist1 were increased in the PDGF-BB group but were significantly decreased in the rapamycin and iCDK9 groups (Fig. 5D). Subsequently, the protein levels of Twist1 were detected, and the results showed that its change trend was consistent with that of the mRNA level (Fig. 5E and F). To further verify that CDK9 can directly regulate the gene levels of Twist1, CDK9 was overexpressed in VSMCs via adenovirus infection, and the protein levels of Twist1 were shown to be significantly increased after CDK9 overexpression (Fig. 5G and H). The current study also employed siCDK9; western blotting showed that, in contrast to overexpression, downregulation of CDK9 by siCDK9 decreased the protein levels of Twist1 in VSMCs (Fig. 5I and J). Furthermore, both the results of the dual-luciferase reporter assay (Fig. 5K) and ChIP-qPCR, in which PDGF-BB increased CDK9 occupancy on the Twist1 promoter (Fig. 5L), demonstrated that CDK9 directly regulated Twist1 gene expression. Overall, these results indicated that CDK9 can regulate the expression levels of Twist1 in VSMCs, which may contribute to its modulatory effects on vascular remodeling.

Harmine alleviates the promoting effect of CDK9 on the proliferation, migration and phenotypic switching of VSMCs. To determine whether Twist1 is required in the CDK9-regulated proliferation and migration of VSMCs, cell proliferation and motility were examined. After being infected with adenovirus (Adv-CDK9 or Adv-Ctrl) for 24 h, VSMCs were treated with the Twist1 inhibitor harmine (20 μM) for another 24 h. Notably, wound healing of VSMCs was significantly promoted by CDK9 overexpression, but this effect was abolished in the presence of harmine (Fig. 6A and B). The inhibitory effect of harmine on VSMC proliferation was further confirmed by EdU incorporation analysis. Consistent with the wound-healing assay results, the number of EdU-positive cells was significantly increased following CDK9 overexpression, but this increase was suppressed by harmine, indicating that Twist1 mediates CDK9-regulated VSMC proliferation (Fig. 6C and D). Consistently, overexpression of CDK9 led to a marked increase in the expression of the proliferation marker PCNA; however, treatment with harmine could reverse this effect, resulting in the inhibition of PCNA expression (Fig. 6E and F). In addition, Twist1 knockdown using siTwist1-5#, the construct with the strongest knockdown among the five screened (Fig. S6), markedly suppressed CDK9 overexpression-induced phenotypic transformation and proliferation of VSMCs, which was verified by detecting contractile markers α-SMA and CNN1, the synthetic marker OPN and the proliferation marker PCNA via western blotting (Fig. 6G).

To further investigate the role of Twist1 in CDK9-regulated phenotypic switching, the inhibition of Twist1 by harmine under PDGF-BB stimulation was explored. PDGF-BB serves a key role in the phenotypic regulation of VSMCs. Thus, VSMCs were pretreated with iCDK9 (2 μM) or harmine (20 μM) for 2 h, followed by incubation with PDGF-BB (20 ng/ml) for 24 h. As expected, both iCDK9 and harmine alone could inhibit PDGF-BB-induced phenotypic switching (Fig. 6H). Notably, harmine could further enhance the inhibitory effect of iCDK9 on PDGF-BB-induced phenotypic switching, leading to a further increase in the expression of

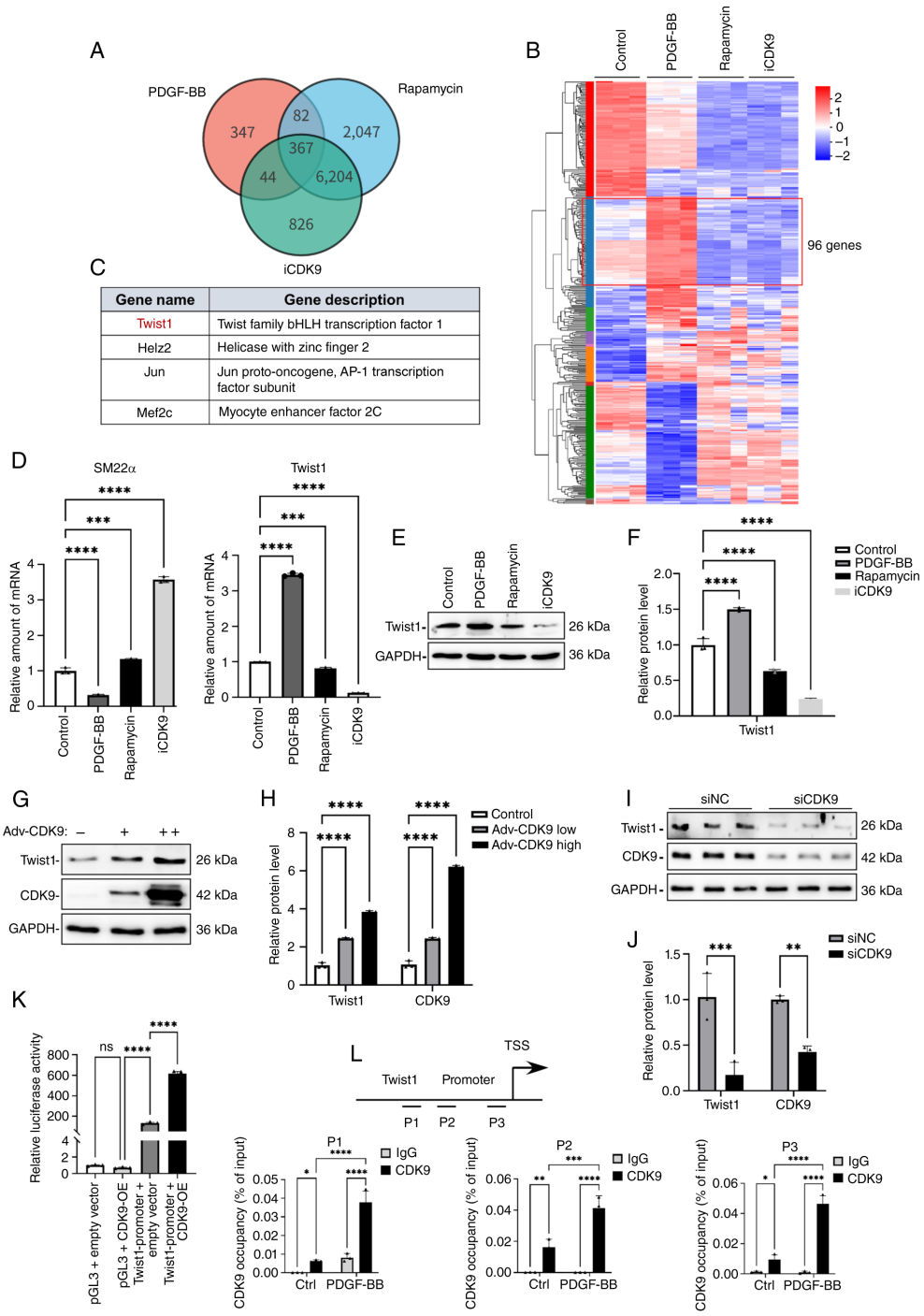


Figure 5. Twist1 is a potential target of CDK9 for regulating phenotypic transformation of smooth muscle cells. (A) RNA sequencing was performed after VSMCs were treated with PDGF-BB, rapamycin or iCDK9 for 24 h. Venn diagram showing changes in transcripts with a rigorous criterion of absolute fold-change ≥2 (|log2FC|≥1) and P<0.05. (B) Heatmap of the 367 genes with significant changes in the PDGF-BB, rapamycin and iCDK9 groups. (C) Four transcription-related genes, Twist1, Helz2, Jun and Mef2c, were identified among the 96 genes that were markedly increased in the PDGF-BB group, but decreased in both the rapamycin and iCDK9 groups. (D) Relative mRNA levels of Twist1 and SM22α, as confirmed by reverse transcription-qPCR. (E) Western blot analysis of Twist1 protein expression in VSMCs after treatment with the indicated agents for 24 h. (F) Semi-quantification of relative Twist1 protein levels after treatment with the indicated agents. Protein expression levels were normalized to GAPDH. (G) Western blot analysis of Twist1 and CDK9 protein expression levels in VSMCs after being infected with Adv-control or Adv-CDK9. (H) Semi-quantification of Twist1 and CDK9 protein expression levels in VSMCs after being infected with Adv-control or Adv-CDK9. Protein expression levels were normalized to GAPDH. (I) Western blot analysis of Twist1 and CDK9 protein expression levels in VSMCs after being transfected with siNC or siCDK9. (J) Semi-quantification of Twist1 and CDK9 protein expression levels in VSMCs after being transfected with siNC or siCDK9. The protein and mRNA expression levels were normalized to GAPDH. (K) Dual-luciferase reporter assay performed in 293T cells. Cells were co-transfected with dual-luciferase reporter plasmids, and relative luciferase activity was quantified as the ratio of firefly luciferase luminescence intensity to *Renilla* luciferase luminescence intensity, with the pGL3-empty vector group set as the control for comparison. (L) Rat SMCs treated with control reagent or PDGF-BB were subjected to ChIP assay with anti-CDK9 antibody. The CDK9 occupancy on the Twist1 promoter at three separate locations was analyzed by qPCR using the primer pairs labeled as P1, P2 and P3 and displayed as percentages of input DNA with the IgG group serving as a negative control. Data are presented as the mean ± SEM. *P<0.05, **P<0.01, ***P<0.001 and ****P<0.0001. Statistical significance was assessed by one- or two-way ANOVA followed by Tukey's post hoc test. All data are from three biological replicates. Adv, adenovirus; CDK9, cyclin-dependent kinase 9; ChIP, chromatin immunoprecipitation; iCDK9, CDK9 inhibitor; NC, negative control; OE, overexpression; qPCR, quantitative PCR; si, small interfering; SM22α, transgelin; TSS, transcription start site; VSMC, vascular smooth muscle cell.

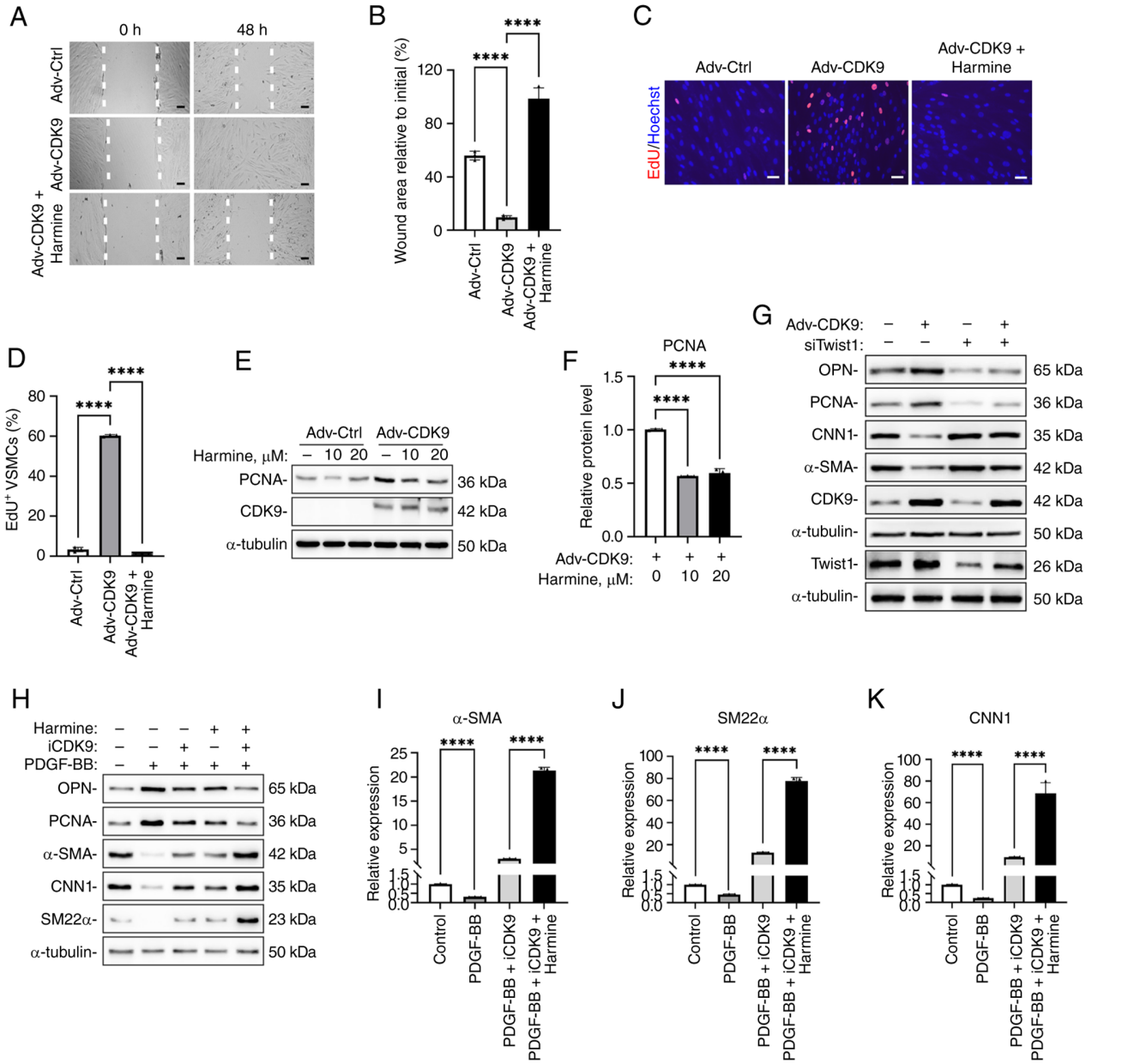


Figure 6. Inhibition of Twist1 alleviates the promoting effect of CDK9 on the proliferation, migration and phenotypic switching of VSMCs. (A) Cell migratory capacity was examined by wound-healing assay in VSMCs, and representative images are shown. Scale bar, 20 μm. (B) Wound area was measured with ImageJ at 48 h and normalized to the 0 h value of the same group, which was set as 100%. (C) Representative images of EdU-positive VSMCs. Scale bar, 20 μm. (D) Quantification of EdU-positive VSMCs. (E) VSMCs were infected with Adv-Ctrl or Adv-CDK9, and, 24 h later, cells were treated with harmine for an additional 24 h. Next, whole cell lysates were subjected to western blot analysis to determine the expression levels of PCNA and CDK9. (F) Semi-quantitative PCNA results after Adv-CDK9 infection with or without harmine treatment, as measured via ImageJ. (G) After being transfected with siNC or siTwist1 for 24 h, VSMCs were infected with Adv-CDK9 for another 24 h, then western blot analysis was performed to assess the indicated proteins. (H) VSMCs were treated with the indicated agents for 24 h, and western blot analysis was then performed to detect the protein levels of OPN, PCNA, α-SMA, CNN1 and SM22α. mRNA levels of (I) α-SMA, (J) SM22α and (K) CNN1 in VSMCs after being treated as indicated for 24 h were determined by reverse transcription-quantitative PCR. Data are presented as the mean ± SEM. ****P<0.0001. Statistical significance was assessed by one-way ANOVA with Tukey's post hoc test; for (I-K), values were log10-transformed since Levene's test indicated unequal variances. All data are from three biological replicates. α-SMA, α-smooth muscle actin; Adv, adenovirus; CDK9, cyclin-dependent kinase 9; CNN1, calponin 1; EdU, 5-ethynyl-2'-deoxyuridine; iCDK9, CDK9 inhibitor; OPN, osteopontin; PCNA, proliferating cell nuclear antigen; PDGF-BB, platelet-derived growth factor-BB; si, small interfering; SM22α, transgelin; VSMC, vascular smooth muscle cell.

contractile markers, including α-SMA, SM22α and CNN1, and a decrease in the expression of the proliferative marker PCNA and the synthetic marker OPN in VSMCs (Fig. 6H). The enhancing effect of harmine on iCDK9-mediated inhibition of VSMC phenotypic switching was further confirmed by RT-qPCR. PDGF-BB significantly reduced the mRNA levels of the contractile markers α-SMA, SM22α and CNN1 relative to the control; following treatment with iCDK9, the reduction was reversed and the introduction of harmine led to a further increase in the expression of these markers (Fig. 6I-K). The results from harmine treatment in the iCDK9-treated and CDK9 overexpression groups showed that harmine was capable of inhibiting CDK9-regulated proliferation, migration and phenotypic switching in VSMCs, and Twist1 may serve as a critical target mediating the regulatory effects of CDK9 on VSMCs.

Discussion

Restenosis remains a major clinical challenge limiting the long-term efficacy of PCI, with neointimal formation driven by abnormal VSMC proliferation, migration and phenotypic switching being its core pathological feature (16,52). The present study systematically investigated the role and molecular mechanism of CDK9 in vascular injury-induced neointimal hyperplasia, and the current findings identified CDK9 as a pivotal regulator of this process, with the transcription factor Twist1 serving as its direct downstream effector.

CDK9 is well characterized for its role in regulating RNA Pol II-dependent gene transcription by phosphorylating the Ser2 residue of the CTD of RNA Pol II (p-Ser2) (31,34). While previous studies have linked CDK9 to cardiovascular diseases, such as AS and PAH (40,41), to the best of our knowledge, its involvement in post-injury neointimal formation remained unaddressed. The current study indicated that CDK9 expression and activity (reflected by p-Ser2 levels) may be significantly upregulated in VSMCs during mouse carotid artery ligation-induced neointimal hyperplasia. These results align with the previous findings that CDK9 regulates VSMC function in AS (41), but extend this knowledge by establishing CDK9/Twist1 axis as a direct contributor to the neointimal response to mechanical vascular injury, which is the primary trigger of PCI restenosis.

A key insight from the present *in vitro* experiments is that CDK9 can modulate multiple VSMC behaviors that are critical for neointimal formation. This is particularly important because phenotypic switching of VSMCs from a quiescent, contractile state to a proliferative, synthetic state is an early and rate-limiting step in neointimal formation (28,31). The present data thus suggested that CDK9 promotes neointimal hyperplasia by coordinately enhancing VSMC proliferation, migration and dedifferentiation, which are three interrelated processes that drive vascular remodeling after injury.

To determine the molecular mechanism by which CDK9 regulates VSMC function, the present study identified Twist1 as the direct target, and the results established a CDK9/Twist1 axis that mediates VSMC dysfunction during neointimal formation. This mechanism expands the current understanding of the transcriptional targets of CDK9 in vascular biology. Prior research has focused on the role of CDK9 in cardiomyocyte hypertrophy via genes such as GATA4 (35), whereas the present study identified Twist1 as a key mediator of the effects of CDK9 on VSMCs. Distinct from earlier studies focusing on AS, the present study focused on a model of vascular injury and neointimal hyperplasia (23,41,42).

The clinical relevance of the present results lies in their potential to address PCI restenosis. The current strategies for restenosis prevention, including drug-eluting stents, have shortcomings, including late stent thrombosis and incomplete inhibition of neointimal growth (12,13). The present study indicated that CDK9 may serve as a potential research target for exploring anti-restenosis strategies; however, a few limitations associated with the current study merit consideration. First, the *in vivo* experiments were conducted exclusively in male mice to avoid the confounding effects of the estrous cycle, which is a common practice in vascular remodeling research. Future studies will include female mice to assess potential sex differences, since sex is a known modifier of cardiovascular disease (4). Second, although attempts were made to generate inducible SMC-specific CDK9-knockout mice in a preliminary experiment of the present study, tamoxifen-induced CDK9 deletion led to severe intestinal enlargement, reduced food intake and premature lethality within ~2 weeks. These animals were euthanized immediately once humane endpoints were reached, and the colony could therefore not be used for the ligation experiments. Therefore, investigating this via genetically engineered models remains technically challenging due to systemic lethality. Another limitation of the current study is that RNA Pol II CTD Ser2 phosphorylation can be mediated not only by CDK9 but also by CDK12 and CDK13. Although the results from CDK9 pharmacological inhibition and chemical-degrader experiments supported that p-Ser2 changes were largely CDK9-dependent in VSMCs under vascular-injury conditions, minor contributions from CDK12/13 cannot be fully excluded. Attempts were made to measure CDK9 autophosphorylation at Thr186 to directly report CDK9 kinase activity; however, multiple commercial p-CDK9 (Thr186) antibodies failed to produce specific and reproducible signals in primary VSMCs and mouse carotid artery tissues (data not shown). Future work utilizing *in vitro* kinase assays may aid in the direct quantification of the intrinsic kinase activity of CDK9. Accordingly, the present study relied on pharmacological inhibition, genetic manipulation, SMC-specific overexpression of CDK9 *in vivo* and adenoviral overexpression to verify the role of CDK9 in neointima formation.

Neointimal hyperplasia-mediated restenosis is an important factor affecting long-term prognosis after PCI intervention. Elucidating the molecular mechanisms underlying VSMC dysfunction will contribute to an improved understanding of vascular remodeling and post-PCI neointimal lesions. The present *in vivo* results showed that pharmacological inhibition of CDK9 can attenuate neointimal hyperplasia, restore the contractile phenotype and suppress excessive VSMC proliferation in a mouse vascular injury model. These preclinical findings provide novel mechanistic insights for understanding the pathogenesis of post-injury neointimal hyperplasia. Consistent alterations of CDK9 expression and VSMC phenotypic transformation in both *in vivo* and *in vitro* models further support the involvement of CDK9 signaling in vascular remodeling. However, since the current study is limited to a mouse carotid ligation model without stent-related injury simulation, long-term safety evaluation or assessment of endothelial repair and thrombotic risk, the translational potential of CDK9 modulation remains to be further verified. Future investigations are required to confirm whether CDK9 can serve as a feasible research target for studying restenosis-related vascular remodeling.

The biological characteristics and potential off-target effects of CDK9 also require further investigation. As a universal transcriptional regulator, CDK9 participates in fundamental physiological functions of multiple normal tissues. Non-specific pharmacological inhibition may disrupt tissue homeostasis and cause unforeseen biological effects. Future basic studies are needed to clarify the tissue-specific regulatory patterns of CDK9 in vascular and non-vascular tissues, to better define its specific function in vascular pathology. Drug-eluting stent coatings enable sustained local

release of iCDK9s, persistently inhibiting excessive activation of the CDK9/Twist1 axis and subsequent vascular restenosis. Such advanced delivery strategies greatly promote the clinical translation of iCDK9-based restenosis therapies. Moreover, this work lacks verification based on clinical samples. Accordingly, further validation in clinical cohorts is required to confirm the association of CDK9/Twist1 expression with restenosis risk. Furthermore, the molecular network downstream of CDK9 in VSMCs requires further clarification. The current study identified Twist1 as a key downstream effector, while additional CDK9-regulated molecules associated with VSMC dysfunction may exist. Multi-omics profiling will help comprehensively delineate the CDK9-mediated signaling network during vascular injury, thereby enriching the mechanistic basis of vascular remodeling research. Furthermore, given the complex and multifactorial nature of restenosis, future basic studies may explore the combined regulatory effects of CDK9 inhibition with other pathological pathways, to further clarify the molecular mechanisms of vascular lesion progression.

In summary, the present study revealed the regulatory role of the CDK9/Twist1 axis in VSMC phenotypic switching and post-injury neointimal hyperplasia, providing novel insights into the basic mechanism of vascular remodeling. All findings are limited to preclinical exploration; therefore, further systematic and in-depth basic research is essential to fully validate and extend the current conclusions.

Acknowledgements

Not applicable.

Funding

The present study was financially supported by the National Natural Science Foundation of China (grant no. 82304578) and the Fujian Provincial Natural Science Foundation (grant no. 2024J011419).

Availability of data and materials

The transcriptomic data generated in the present study may be found in the Sequence Read Archive (National Center for Biotechnology Information) database under accession number PRJNA1357582 or at the following URL: https://www.ncbi.nlm.nih.gov/bioproject/PRJNA1357582. The other data generated in the present study may be requested from the corresponding author.

Authors' contributions

GL and JW designed the research and wrote the article. LY, XZ, JC and ML performed the experiments. RW analyzed the data. LY and JW confirm the authenticity of all the raw data. All authors read and approved the final manuscript.

Ethics approval and consent to participate

All animal procedures were approved by the Institutional Animal Care and Use Committee of Xiamen University (approval no. XMULAC20250055; Xiamen, China). The primary human aortic smooth muscle cells used in the present study were commercially obtained and derived from anonymized human tissues; no human tissue was collected or isolated by our research team. The use of these cells for *in vitro* experiments was granted an ethical exemption by the Institutional Ethics Committee of Xiamen Cardiovascular Hospital, Xiamen University.

Patient consent for publication

Not applicable.

Competing interests

The authors declare that they have no competing interests.

References

1. DALYs GBD and Collaborators H: Global, regional, and national disability-adjusted life-years (DALYs) for 359 diseases and injuries and healthy life expectancy (HALE) for 195 countries and territories, 1990-2017: A systematic analysis for the Global Burden of Disease Study 2017. Lancet 392: 1859-1922, 2018.
2. Lavie CJ: Progress in cardiovascular diseases statistics 2022. Prog Cardiovasc Dis 73: 94-95, 2022.
3. Fairweather D, Aung N and Carter RE: Editorial: Novel translational advances in artificial intelligence for diagnosis and treatment of cardiovascular diseases. Front Cardiovasc Med 12: 1604528, 2025.
4. Goodarzynejad H, Sheikh Fathollahi M and Shafiee A: Editorial: The role of sex in coronary artery disease. Front Cardiovasc Med 10: 1220439, 2023.
5. Anderson LL, Dai D, Miller AL, Roe MT, Messenger JC and Wang TY: Percutaneous coronary intervention for older adults who present with syncope and coronary artery disease? Insights from the National Cardiovascular Data Registry. Am Heart J 176: 1-9, 2016.
6. Lawrie K, O'Neill S, Malik J, Balaz P, Corr M and Waldauf P: Classifications of haemodialysis vascular access-induced limb ischaemia. J Vasc Access 27: 52-62, 2026.
7. Tachi M, Tanaka A, Riku S, Furuta T, Tobe A, Hayashi K and Murohara T: Percutaneous treatment for venous stenosis caused by a vascular closure device. Cardiovasc Revasc Med 40S: 157-158, 2022.
8. Serruys PW, Ono M, Garg S, Hara H, Kawashima H, Pompilio G, Andreini D, Holmes DR Jr, Onuma Y and King Iii SB: Percutaneous coronary revascularization: JACC historical breakthroughs in perspective. J Am Coll Cardiol 78: 384-407, 2021.
9. Chacko L, P Howard J, Rajkumar C, Nowbar AN, Kane C, Mahdi D, Foley M, Shun-Shin M, Cole G, Sen S, *et al*: Effects of percutaneous coronary intervention on death and myocardial infarction stratified by stable and unstable coronary artery disease: A Meta-analysis of randomized controlled trials. Circ Cardiovasc Qual Outcomes 13: e006363, 2020.
10. Akbari T and Al-Lamee R: Percutaneous coronary intervention in Multi-vessel disease. Cardiovasc Revasc Med 44: 80-91, 2022.
11. Watanabe H, Yamamoto K, Shiomi H, Morimoto T, Kato E, Matsumura Y, Nakatsuma K, Takeji Y, Yaku H, Yamamoto E, *et al*: Percutaneous coronary intervention using new-generation drug-eluting stents versus coronary arterial bypass grafting in stable patients with multi-vessel coronary artery disease: From the CREDO-Kyoto PCI/CABG registry Cohort-3. PLoS One 17: e0267906, 2022.
12. Fattori R and Piva T: Drug-eluting stents in vascular intervention. Lancet 361: 247-249, 2003.
13. McNair ED, Wells CR, Mabood Qureshi A, Basran R, Pearce C, Orvold J, Devilliers J and Prasad K: Soluble receptors for advanced glycation end products (sRAGE) as a predictor of restenosis following percutaneous coronary intervention. Clin Cardiol 33: 678-685, 2010.
14. Zhao L, Feng L, Shan R, Huang Y, Shen L, Fan M and Wang Y: Nanoparticle-based approaches for treating restenosis after vascular injury. Front Pharmacol 15: 1427651, 2024.

15. Xu K, Al-Ani MK, Pan X, Chi Q, Dong N and Qiu X: Plant-derived products for treatment of vascular intima hyperplasia selectively inhibit vascular smooth muscle cell functions. Evid Based Complement Alternat Med 2018: 3549312, 2018.
16. Owens GK, Kumar MS and Wamhoff BR: Molecular regulation of vascular smooth muscle cell differentiation in development and disease. Physiol Rev 84: 767-801, 2004.
17. Zhang Q, Li H, Zhuang T, Xu L, Wu W, Pi J, Zhu P, Geng L, Duan Y, Xu J, *et al*: CCN5 suppresses injury-induced vascular restenosis by inhibiting smooth muscle cell proliferation and facilitating endothelial repair via thymosin beta4 and Cd9 pathway. Eur Heart J 46: 1645-1658, 2025.
18. Lacolley P, Regnault V, Nicoletti A, Li Z and Michel JB: The vascular smooth muscle cell in arterial pathology: A cell that can take on multiple roles. Cardiovasc Res 95: 194-204, 2012.
19. Frismantiene A, Philippova M, Erne P and Resink TJ: Smooth muscle cell-driven vascular diseases and molecular mechanisms of VSMC plasticity. Cell Signal 52: 48-64, 2018.
20. Mao C, Ma Z, Jia Y, Li W, Xie N, Zhao G, Ma B, Yu F, Sun J, Zhou Y, *et al*: Nidogen-2 maintains the contractile phenotype of vascular smooth muscle cells and prevents neointima formation via bridging Jagged1-Notch3 signaling. Circulation 144: 1244-1261, 2021.
21. Chen R, McVey DG, Shen D, Huang X and Ye S: Phenotypic switching of vascular smooth muscle cells in atherosclerosis. J Am Heart Assoc 12: e031121, 2023.
22. Yap C, Mieremet A, de Vries CJM, Micha D and de Waard V: Six shades of vascular smooth muscle cells illuminated by KLF4 (Kruppel-Like Factor 4). Arterioscler Thromb Vasc Biol 41: 2693-2707, 2021.
23. Basatemur GL, Jorgensen HF, Clarke MCH, Bennett MR and Mallat Z: Vascular smooth muscle cells in atherosclerosis. Nat Rev Cardiol 16: 727-744, 2019.
24. Grootaert MOJ and Bennett MR: Vascular smooth muscle cells in atherosclerosis: Time for a re-assessment. Cardiovasc Res 117: 2326-2339, 2021.
25. Farina FM, Hall IF, Serio S, Zani S, Climent M, Salvarani N, Carullo P, Civilini E, Condorelli G, Elia L and Quintavalle M: miR-128-3p is a novel regulator of vascular smooth muscle cell phenotypic switch and vascular diseases. Circ Res 126: e120-e135, 2020.
26. Zhao C, Shen J, Lu Y, Ni H, Xiang M and Xie Y: Dedifferentiation of vascular smooth muscle cells upon vessel injury. Int Immunopharmacol 144: 113691, 2025.
27. Jensen LF, Bentzon JF and Albarran-Juarez J: The phenotypic responses of vascular smooth muscle cells exposed to mechanical cues. Cells 10: 2209, 2021.
28. Cao G, Xuan X, Hu J, Zhang R, Jin H and Dong H: How vascular smooth muscle cell phenotype switching contributes to vascular disease. Cell Commun Signal 20: 180, 2022.
29. Chappell J, Harman JL, Narasimhan VM, Yu H, Foote K, Simons BD, Bennett MR and Jørgensen HF: Extensive proliferation of a subset of differentiated, yet plastic, medial vascular smooth muscle cells contributes to neointimal formation in mouse injury and atherosclerosis models. Circ Res 119: 1313-1323, 2016.
30. Suna G, Wojakowski W, Lynch M, Barallobre-Barreiro J, Yin X, Mayr U, Baig F, Lu R, Fava M, Hayward R, *et al*: Extracellular matrix proteomics reveals interplay of aggrecan and aggrecanases in vascular remodeling of stented coronary arteries. Circulation 137: 166-183, 2018.
31. Paparidis NF, Durvale MC and Canduri F: The emerging picture of CDK9/P-TEFb: More than 20 years of advances since PITALRE. Mol Biosyst 13: 246-276, 2017.
32. Zheng B, Gold S, Iwanaszko M, Howard BC, Wang L and Shilatifard A: Distinct layers of BRD4-PTEFb reveal bromodomain-independent function in transcriptional regulation. Mol Cell 83: 2896-2910.e4, 2023.
33. Larochelle S, Amat R, Glover-Cutter K, Sansó M, Zhang C, Allen JJ, Shokat KM, Bentley DL and Fisher RP: Cyclin-dependent kinase control of the initiation-to-elongation switch of RNA polymerase II. Nat Struct Mol Biol 19: 1108-1115, 2012.
34. Zhou Q, Li T and Price DH: RNA polymerase II elongation control. Annu Rev Biochem 81: 119-143, 2012.
35. Sunagawa Y, Morimoto T, Takaya T, Kaichi S, Wada H, Kawamura T, Fujita M, Shimatsu A, Kita T and Hasegawa K: Cyclin-dependent kinase-9 is a component of the p300/GATA4 complex required for phenylephrine-induced hypertrophy in cardiomyocytes. J Biol Chem 285: 9556-9568, 2010.
36. Sano M, Abdellatif M, Oh H, Xie M, Bagella L, Giordano A, Michael LH, DeMayo FJ and Schneider MD: Activation and function of cyclin T-Cdk9 (positive transcription elongation factor-b) in cardiac muscle-cell hypertrophy. Nat Med 8: 1310-1317, 2002.
37. Li Z, Guo Z, Lan R, Cai S, Lin Z, Li J, Wang J, Li Z and Liu P: The poly(ADP-ribosyl)ation of BRD4 mediated by PARP1 promoted pathological cardiac hypertrophy. Acta Pharm Sin B 11: 1286-1299, 2021.
38. Matrone G, Wilson KS, Maqsood S, Mullins JJ, Tucker CS and Denvir MA: CDK9 and its repressor LARP7 modulate cardiomyocyte proliferation and response to injury in the zebrafish heart. J Cell Sci 128: 4560-4571, 2015.
39. Xue Q, Zhang Q, Guo Z, Wu L, Chen Y, Chen Z, Yang K and Cao J: Therapeutic Hypothermia Inhibits Hypoxia-Induced Cardiomyocyte Apoptosis Via the MiR-483-3p/Cdk9 Axis. J Am Heart Assoc 12: e026160, 2023.
40. Jia Q, Hu Z, Song N and Mao W: Flavopiridol mitigates the progression of Monocrotaline-induced pulmonary hypertension in rats by targeting Cyclin-dependent kinase 9. Cardiovasc Drugs Ther 37: 449-460, 2023.
41. Huang S, Luo W, Wu G, Shen Q, Zhuang Z, Yang D, Qian J, Hu X, Cai Y, Chattipakorn N, *et al*: Inhibition of CDK9 attenuates atherosclerosis by inhibiting inflammation and phenotypic switching of vascular smooth muscle cells. Aging (Albany NY) 13: 14892-14909, 2021.
42. Han Y, Zhao S, Gong Y, Hou G, Li X and Li L: Serum cyclin-dependent kinase 9 is a potential biomarker of atherosclerotic inflammation. Oncotarget 7: 1854-1862, 2016.
43. Kimura Y, Izumiya Y, Araki S, Yamamura S, Hanatani S, Onoue Y, Ishida T, Arima Y, Nakamura T, Yamamoto E, *et al*: Sirt7 deficiency attenuates neointimal formation following vascular injury by modulating vascular smooth muscle cell proliferation. Circ J 85: 2232-2240, 2021.
44. Livak KJ and Schmittgen TD: Analysis of relative gene expression data using real-time quantitative PCR and the 2(-Delta Delta C(T)) method. Methods 25: 402-408, 2001.
45. Wu J, Xue Y, Gao X and Zhou Q: Host cell factors stimulate HIV-1 transcription by antagonizing substrate-binding function of Siah1 ubiquitin ligase to stabilize transcription elongation factor ELL2. Nucleic Acids Res 48: 7321-7332, 2020.
46. Xu Y, Ma X, Ni W, Zheng L, Lin Z, Lai Y, Yang N, Dai Z, Yao T, Chen Z, *et al*: PKM2-driven lactate overproduction triggers Endothelial-To-Mesenchymal transition in ischemic flap via mediating TWIST1 Lactylation. Adv Sci (Weinh) 11: e2406184, 2024.
47. Yu X, He T, Tong Z, Liao L, Huang S, Fakhouri WD, Edwards DP and Xu J: Molecular mechanisms of TWIST1-regulated transcription in EMT and cancer metastasis. EMBO Rep 24: e56902, 2023.
48. Tu M, Ge B, Li J, Pan Y, Zhao B, Han J, Wu J, Zhang K, Liu G, Hou M, *et al*: Emerging biological functions of Twist1 in cell differentiation. Dev Dyn 254: 8-25, 2025.
49. Wang Y, Yang K, Jiang G, Zheng X, Cheng F and Li W: Twist1 promoting neointima hyperplasia after vascular injury in diabetes via regulating hyperglycemia-induced phenotype switching of vascular smooth muscle cells. Atherosclerosis 409: 120496, 2025.
50. Ren J, Xiao X, Li R, Lv C, Zhang Y, Wang L, Hong T, Zhang H and Wang Y: Single-cell sequencing reveals that endothelial cells, EndMT cells and mural cells contribute to the pathogenesis of cavernous malformations. Exp Mol Med 55: 628-642, 2023.
51. Fan Y, Gu X, Zhang J, Sinn K, Klepetko W, Wu N, Foris V, Solymosi P, Kwapiszewska G and Kuebler WM: TWIST1 drives smooth muscle cell proliferation in pulmonary hypertension via loss of GATA-6 and BMPR2. Am J Respir Crit Care Med 202: 1283-1296, 2020.
52. Yang G, Zhang Z, Ma X, Chen J, Shi H, Yang J and Han Q Role of carvedilol in inhibiting the proliferation and migration of vascular smooth muscle cells by upregulating microRNA-145 expression. Physiol Res 74: 577-588, 2025.

Copyright © 2026 Yu et al. This work is licensed under a Creative Commons Attribution-NonCommercial-NoDerivatives 4.0 International (CC BY-NC-ND 4.0) License.